Electronic Supplementary Material (ESI) for Materials Horizons.

Supporting Information

Scalable Multi-Dimensional Topological Deformation Actuators for Active Object Identification

Tianyi Ji, Wei Gong,* Jie Zhou, Yangmin Jing, Ruizhe Xing, Bingjie Zhu, Kerui Li, Chengyi Hou,* Qinghong Zhang, Yaogang Li,* Hongzhi Wang

List of Contents

different bending effects.

Figure S15. DSC heating scan and DSC cooling scan of LDPE.

Figure S16. Digital photo of surface potential test experiment.

Figure S17. The triboelectric signals generated by TDA when grasping small size, medium size, and large size target objects.

Table S1. The average motion parameters in the MD and the TD of actuators made of LDPE with different orientation factors.

Table S2. Track coordinates of the four vertexes of the TDA in the three-dimensional space during deformation.

Video S1. FEA model of flow velocity of compressed gas in LDPE balloon during blow molding.

Video S2. Preparation of large-scale TDA by industrial scraping machine.

Video S3. The deformation of the actuator in sunlight.

Video S4. The actuator acts as a robot to crawl quickly in the sunlight.

Video S5. The deformation of the actuator made at 45 °C.

Video S6. Topological deformation of the TDA when cutting along the orientation direction.

Video S7. Topological deformation of the TDA when cutting along a 45° angle to the orientation direction.

Video S8. FEA model of TDA deformation with temperature change.

Supplemental Figures

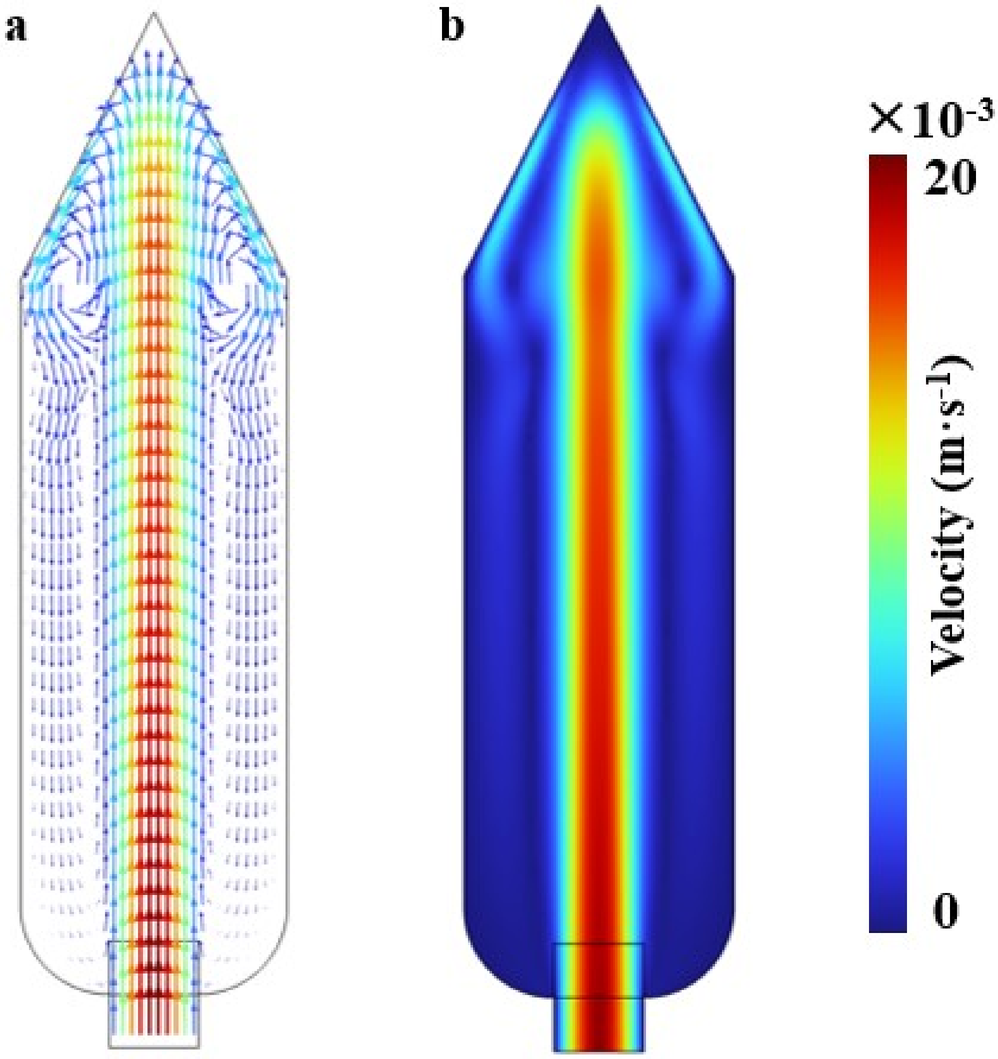

Figure S1. FEA model of flow velocity of compressed gas in LDPE balloon during blow molding. (a) Air flow direction. (b) Air velocity field.

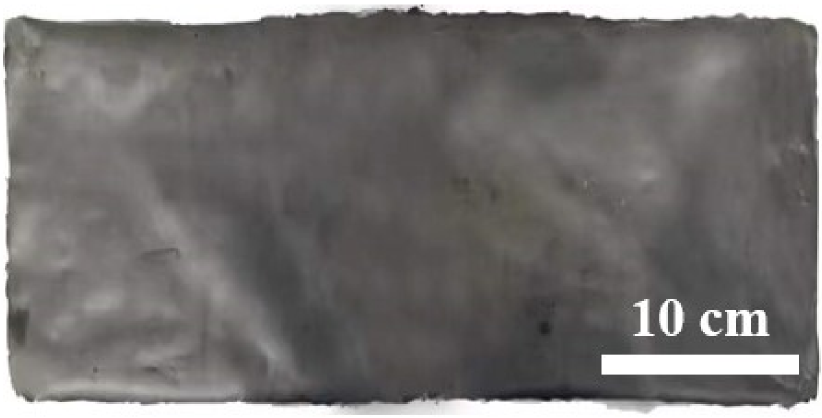

Figure S2. Digital photograph of the actuator with a large size.

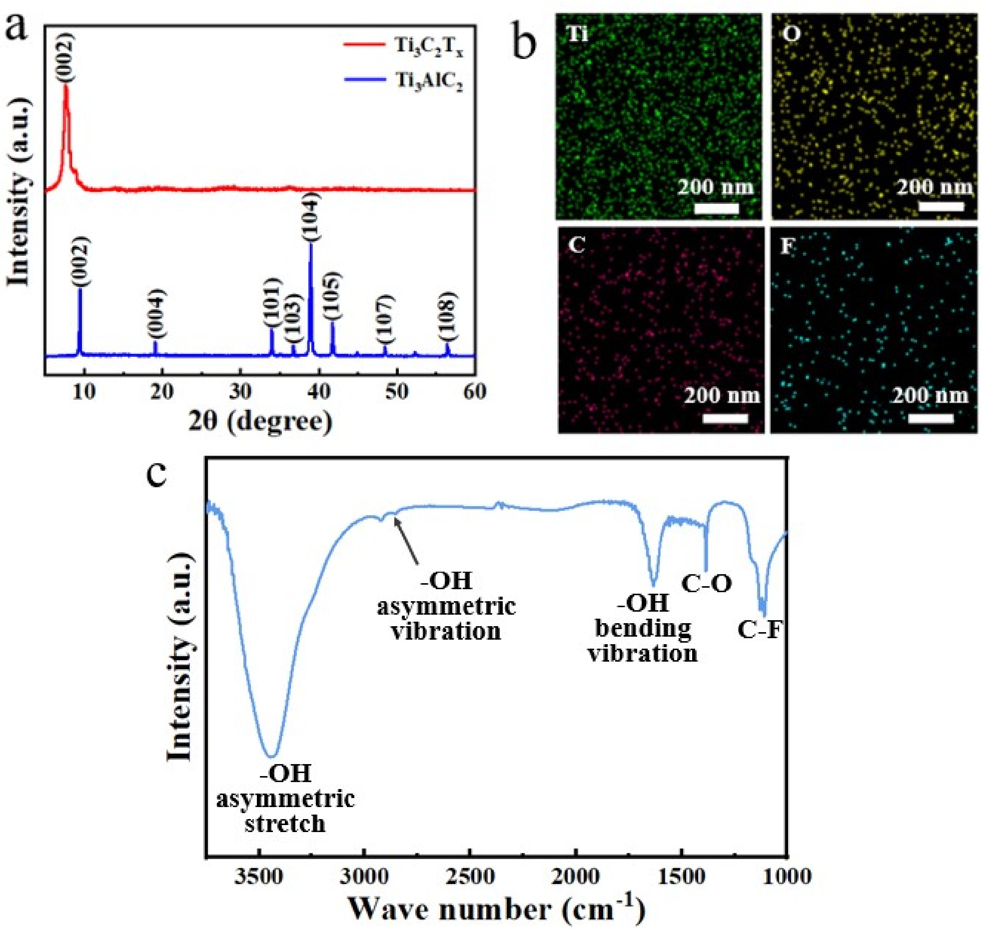

Figure S3. Characterization test of MXene. (a) XRD patterns of MXene and its MAX phase. (b) Elemental mapping of Ti, O, C, and F. (c) FT-IR spectra of MXene.

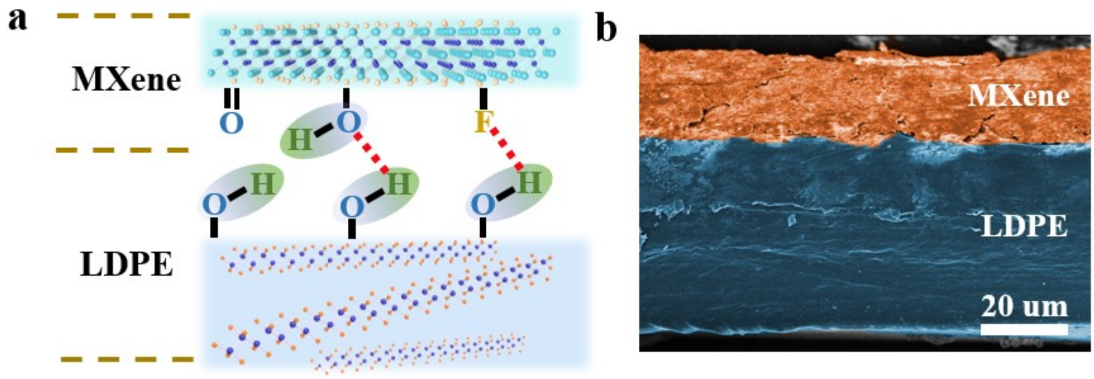

Figure S4. The tight adhesion between the two layers of the actuator. (a) Schematic diagram of hydrogen bond between two structural layers of the actuator. (b) Cross-sectional SEM image of the actuator.

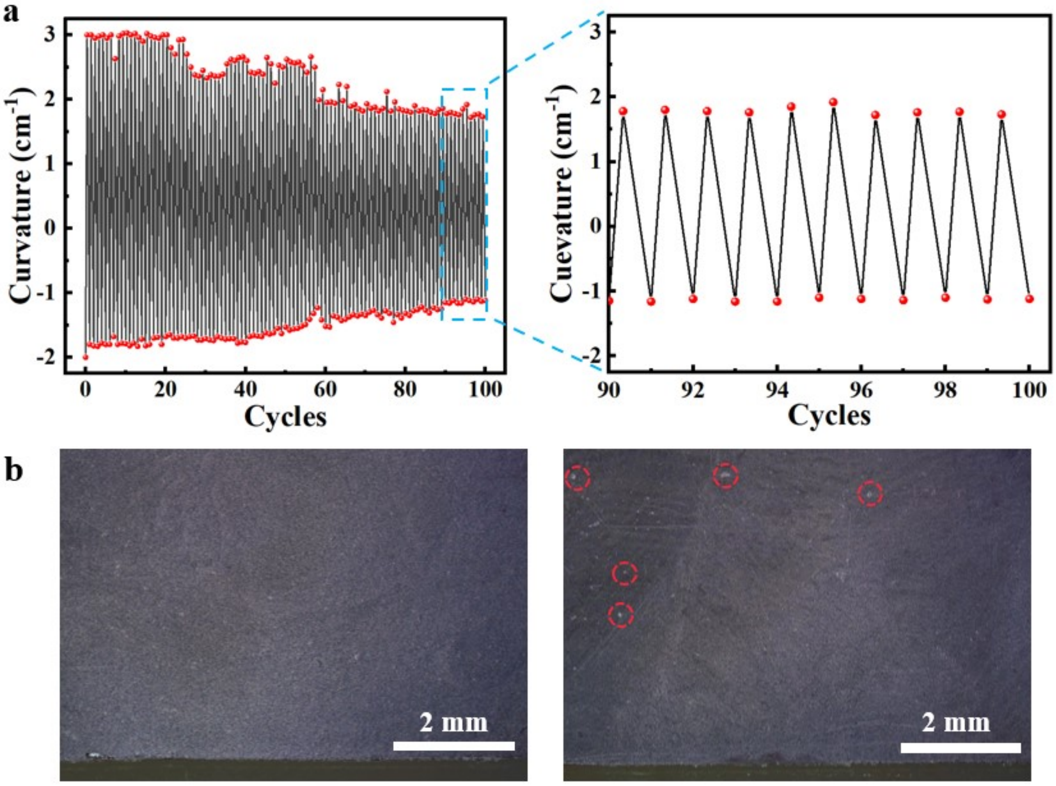

Figure S5. Durability test of the TDA. (a) The TDA deformation curvature was maximized under the driving of infrared light, and it was continuously operated to carry out durability test. After the actuator had operated for 100 cycles, its actuating performance decayed to about 60% of the initial value. (b) Super-depth pictures of the TDA before (left) and after (right) 100 cycles of deformation. After 100 times of deformation, the surface of the TDA did not crack and fall off of MXene, but was only stained with a little dust (shown by the red circle). The decrease of the deformation ability of the TDA was attributed to the aging of LDPE during frequent heating and cooling, and its mechanical properties were reduced.

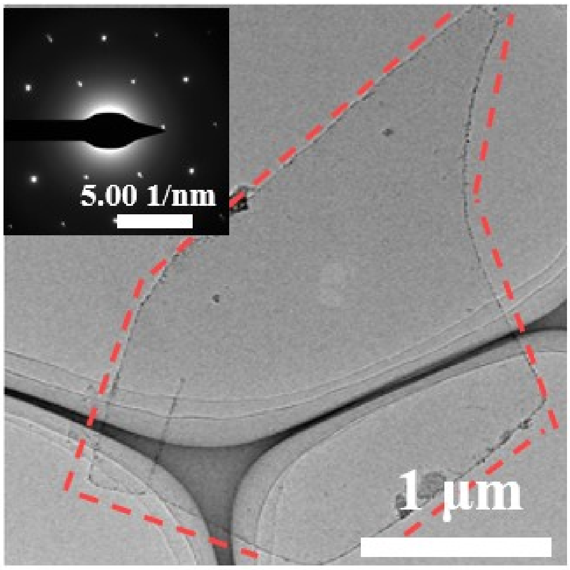

Figure S6. TEM image of small-sized MXene nanosheet etched by highly concentrated hydrofluoric acid, and the inset is the SAED pattern.

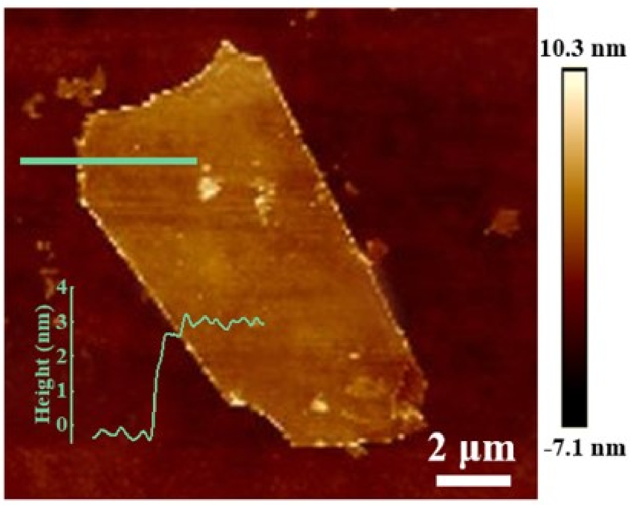

Figure S7. AFM image of the MXene nanosheet, the inset is the height profile measured along the solid line. The average thickness of the nanosheet is 2.8 nm, indicating that MXene is peeled into two layers or less theoretically. In fact, MXene will coordinate various functional groups on its surface during the etching process, which will make the actual thickness of the nanosheet greater than the theoretical value.

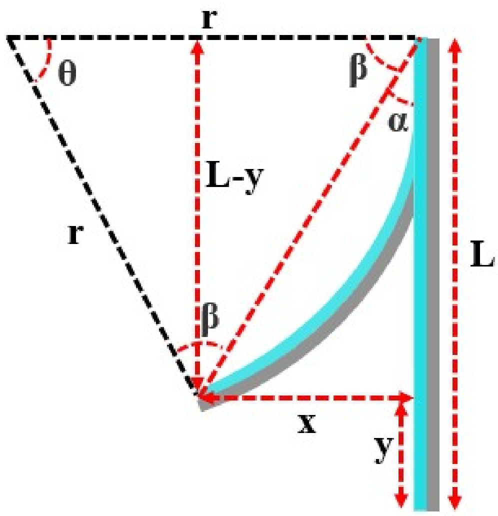

Figure S8. Parameters used to calculate curvature during actuator deformation.

L: Total length of the actuator.

r: Radius of curvature during the actuator bending.

x: Displacement in horizontal direction during the actuator bending.

y: Displacement in vertical direction during the actuator bending.

θ: Bending angle of the arc of the actuator.

α: Included angle between the connecting line at both ends of the actuator and the vertical direction during bending.

β: Two angles β are the other two angles of the isosceles triangle where angle θ is located.

Angle α is deduced as

$$\alpha = \frac{1}{tan[\frac{x}{L-y}]}$$

Angle β is also the remainder of angle α, so the following equation exists

$$\frac{\pi - \theta}{2} = \frac{\pi}{2} - \frac{\theta}{2} = \beta = \frac{\pi}{2} - \alpha$$

$$\theta = 2\alpha$$

As the bending angle is given by

$$\theta = \frac{L}{r}$$

The curvature C is deduced as

$$C = \frac{1}{r} = \frac{\theta}{L} = \frac{2\alpha}{L} = \frac{2}{Ltan[\frac{x}{L-y}]}$$

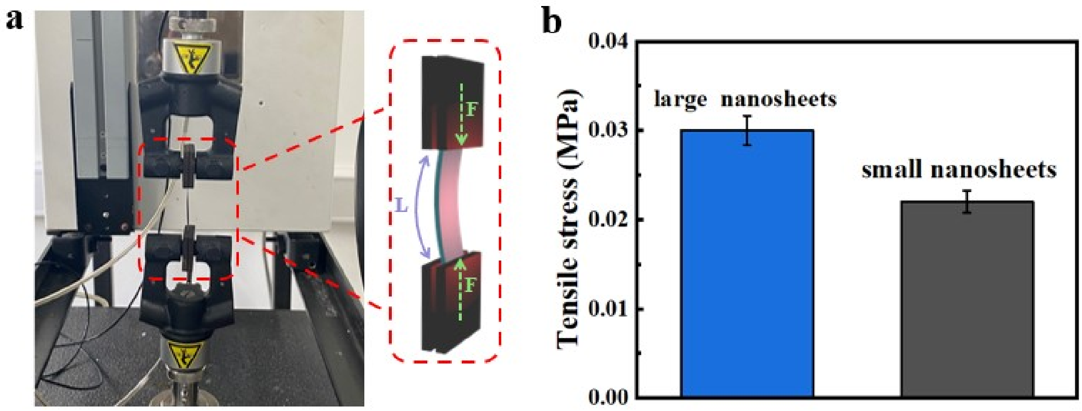

Figure S9. Testing of actuator deformation force. (a) The force generated by the actuator were measured on the universal testing machine with on/off NIR light irradiations. (b) Deformation force data of actuators made of large-sized and small-sized MXene nanosheets respectively.

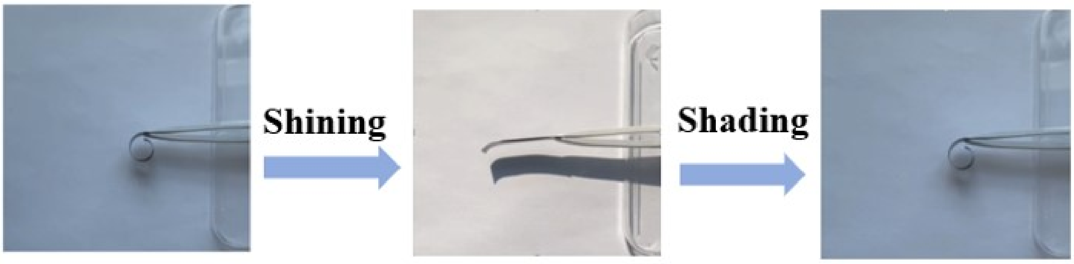

Figure S10. Deformation of the actuator in sunlight. The actuator can be bent or straightened with or without the influence of sunlight by manually opening and closing the light shielding window.

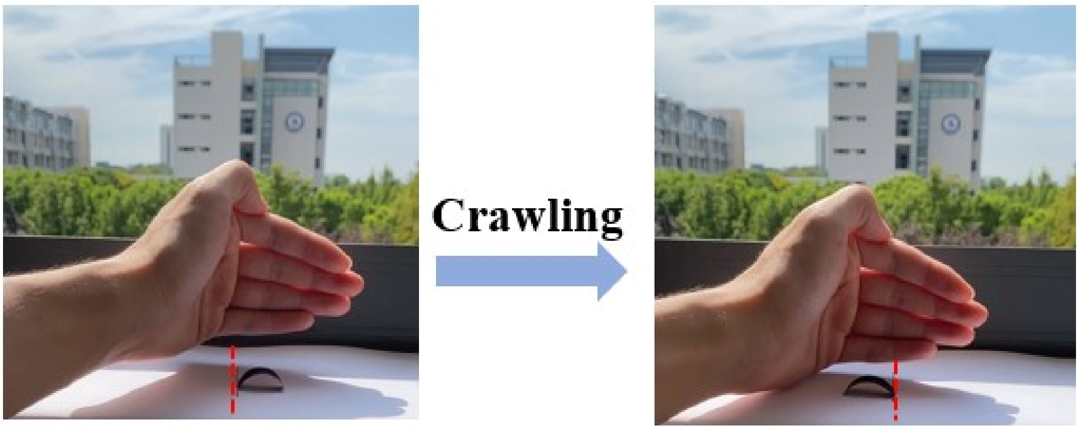

Figure S11. The actuator crawls in the sun. By periodically blocking the sunlight, the actuator can quickly crawl for one body distance.

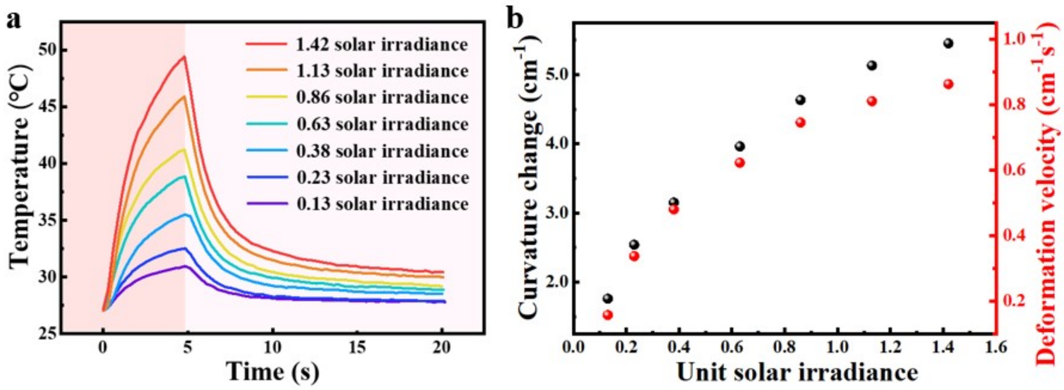

Figure S12. Temperature changes (a) and actuating performances (b) of the TDA under natural light with different light intensities. As we can see from Figure S12a, the TDA can obviously heat up under the light whose intensity is weaker than the unit solar irradiance, and the heating rate increases with the increase of light intensity. The curvature changes and deformation velocity of the TDA increase with the increase of the illumination intensity as well (Figure S12b). It is worth noting that the TDA still has deformation behavior even under the light with intensity as weak as 0.12 solar irradiance.

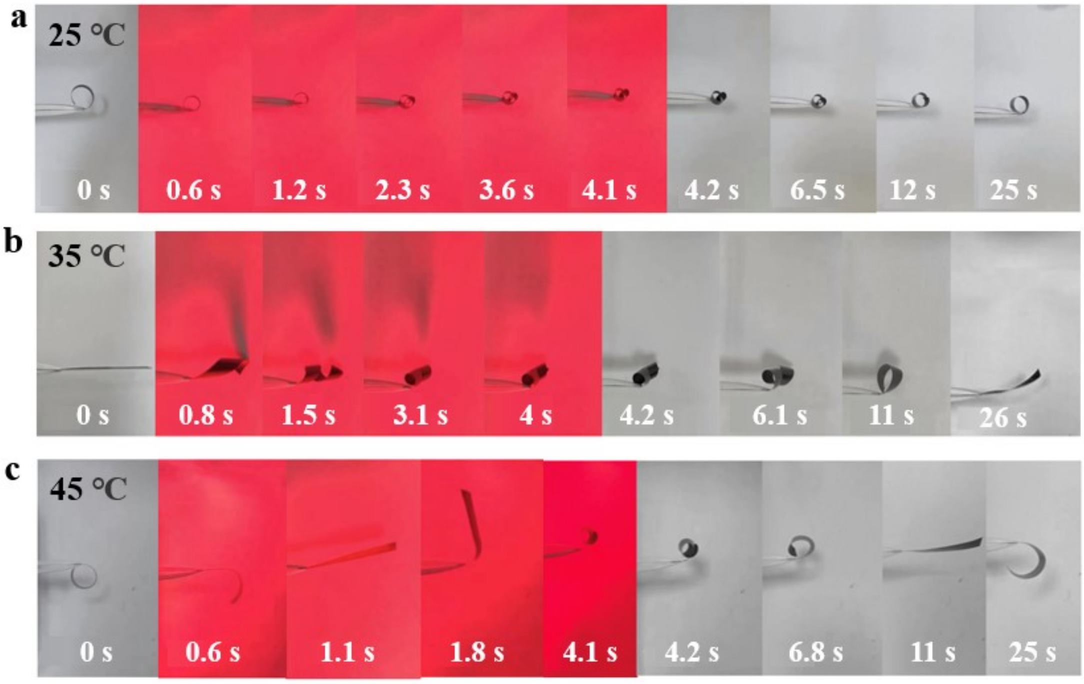

Figure S13. Digital photos of actuation of actuators made at different molding temperatures. (a) The deformation that always maintains positive curvature. (b) The deformation from zero curvature to positive curvature. (c) Deformation from negative curvature to positive curvature.

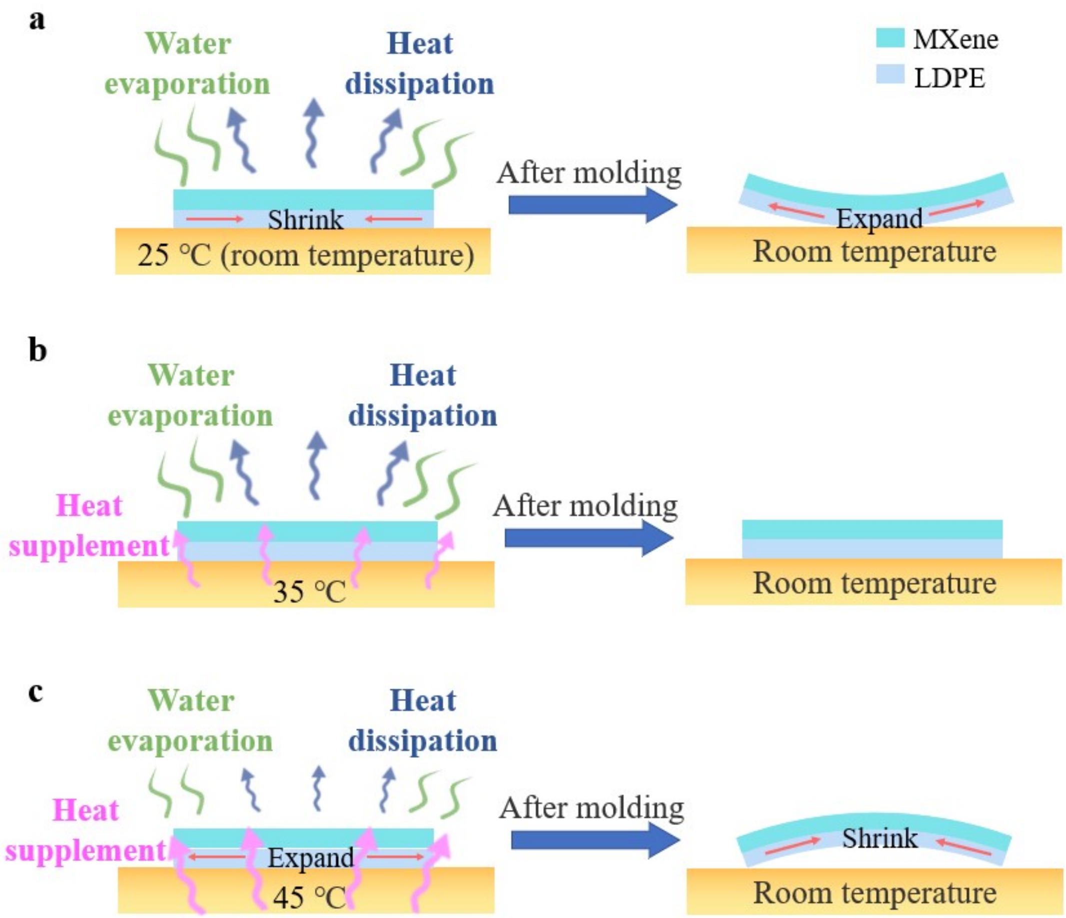

Figure S14. Principle of forming actuators at different temperatures to obtain different bending effects. (a) The initial positive curvature of the actuator is achieved by evaporation of water from the MXene layer during the forming process. (b) The initial zero curvature of the actuator is obtained by counteracting the evaporation and heating during the forming process. (c) The initial negative curvature of the actuator is achieved by heating from hot table.

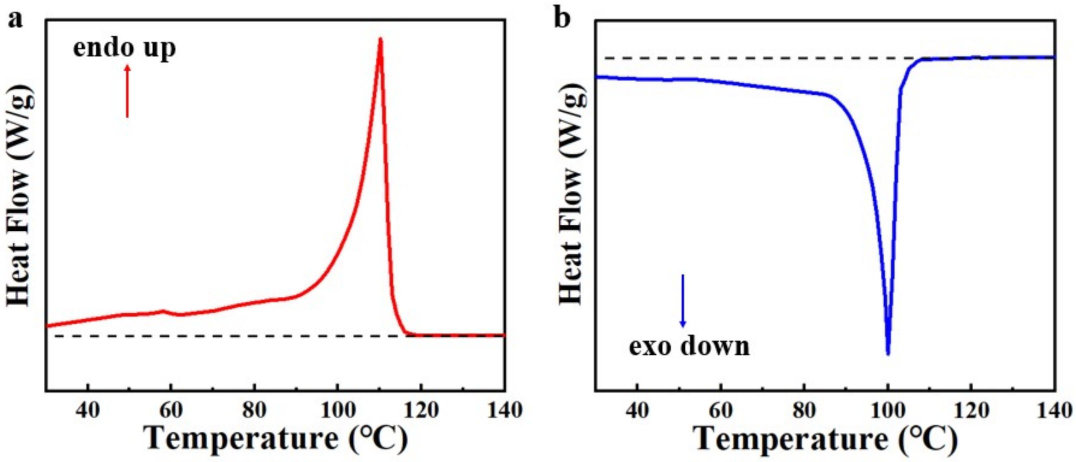

Figure S15. DSC heating scan (a) and DSC cooling scan (b) of LDPE. It can be seen from Figure S13a that there is a wide melting range before the melting peak of LDPE at about 110 ℃. In particular, there is a small melting peak near 58 ℃. The above phenomenon is due to the wide molecular weight distribution of LDPE and some imperfect crystal regions in the production process, which will melt at a lower temperature. Correspondingly, the crystallinity of LDPE also increases slightly during the cooling process.

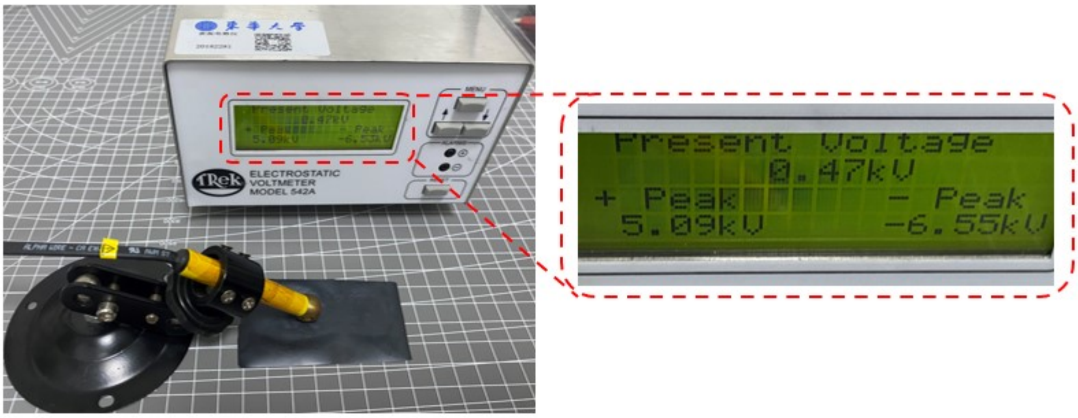

Figure S16. Digital photo of surface potential test experiment. After TDA grabs the object, use the probe of surface potentiometer to test its surface potential.

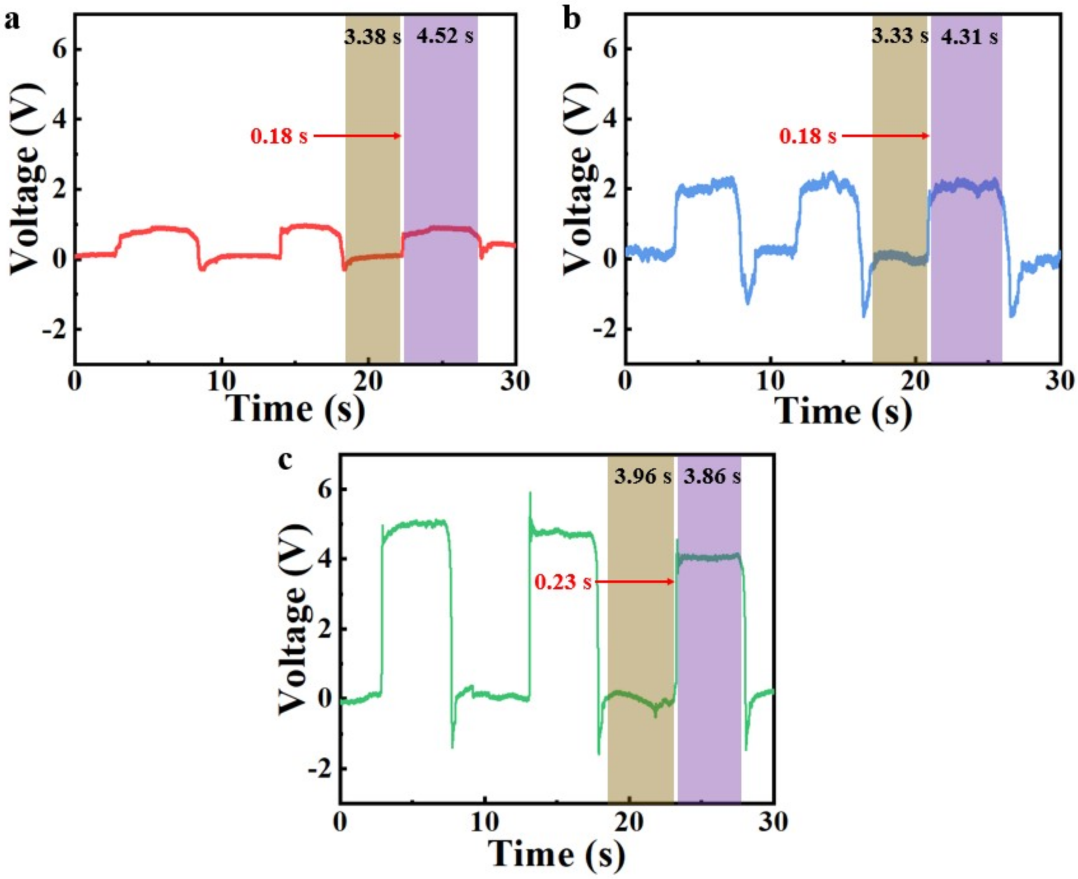

Figure S17. The triboelectric signals generated by the TDA when grasping small size (a), medium size (b), and large size (c) target objects. The brown areas in the figures represent the deformation processes of TDA, while the purple areas represent the processes of TDA clamping the target objects, and the white areas between the two represent the response time of object identification. The fastest response time for TDA's object identification is 0.18 s.

Supplemental Tables

Table S1. The average motion parameters in the MD and the TD of actuators made of LDPE with different orientation factors.

	Curvature in MD (cm^{-1})	Force in MD (Mpa)	Velocity in MD ($cm^{-1}s^{-1}$)	Curvature in TD (cm^{-1})	Force in TD (Mpa)	Velocity in TD ($cm^{-1}s^{-1}$)
$f = 0.24$	0.4	0.01	0.2	0.35	0.01	0.2
$f = 0.38$	0.8	0.018	0.37	0.41	0.012	0.2
$f = 0.61$	2	0.03	1.13	1.6	0.03	0.98
$f = 0.72$	2.5	0.034	1.16	0.3	0.012	0.35
$f = 0.80$	2.8	0.035	1.2	/	/	/

Table S2. Track coordinates of the four vertexes of the TDA in the three-dimensional space during deformation. (Take the TDA with side length of 60 mm as an example.)

	α	β	γ	δ
State 1	(30, -30, -3)	(30, -30, 0)	(30, 30, 0)	(30, 30, -3)
State 2	(42.7, -30, -12.7)	(30, -30, 0)	(30, 30, 0)	(42.7, 30, -12.7)
State 3	(30, -30, -38.2)	(30, -30, 0)	(30, 30, 0)	(30, 30, -38.2)
State 4	(-8.2, -30, -38.2)	(30, -30, 0)	(30, 30, 0)	(-8.2, 30, -38.2)
State 5	(-24, -30, -18)	(30, -30, 0)	(30, 30, 0)	(-24, 30, -18)
State 6	(-30, -30, 0)	(30, -30, 0)	(30, 30, 0)	(-30, 30, 0)
State 7	(-30, -27, 9)	(30, -27, 9)	(30, 27, 9)	(-30, 27, 9)
State 8	(-30, -21, 16)	(30, -21, 16)	(30, 21, 16)	(-30, 21, 16)
State 9	(-30, -13, 16)	(30, -13, 16)	(30, 13, 16)	(-30, 13, 16)